Carbohydrate Polymers 101 (2014) 1225–1233

Contents lists available at ScienceDirect

Carbohydrate Polymers

journal homepage: www.elsevier.com/locate/carbpol

Dextran sulfate-coated superparamagnetic iron oxide nanoparticles as a contrast agent for atherosclerosis imaging

Dong Gil You[a,b,1], Gurusamy Saravanakumar[a,1], Soyoung Son[a], Hwa Seung Han[a], Roun Heo[c], Kwangmeyung Kim[b], Ick Chan Kwon[b], Jun Young Lee[a], Jae Hyung Park[a,c,*]

[a] Departments of Polymer Science and Chemical Engineering, College of Engineering, Sungkyunkwan University, Suwon 440-746, Republic of Korea
[b] Center for Theragnosis, Biomedical Research Institute, Korea Institute of Science and Technology (KIST), Hwarangno 14-gil 6, Seongbuk-gu, Seoul 136-791, Republic of Korea
[c] Department of Health Sciences and Technology, SAIHST, Sungkyunkwan University, Suwon 440-746, Republic of Korea

ARTICLE INFO

Article history:
Received 14 May 2013
Received in revised form
16 September 2013
Accepted 21 October 2013
Available online 26 October 2013

Keywords:
Dextran sulfate
Atherosclerosis
Double hydrophilic copolymer
Contrast agent
Magnetic resonance imaging

ABSTRACT

The hallmark of atherosclerosis in its early pathogenic process is the overexpression of class A scavenger receptors (SR-A) by activated macrophages. In this study, dextran sulfate-coated superparamagnetic iron oxide nanoparticles (DS-SPIONs), as a magnetic resonance (MR) imaging contrast agent of atherosclerosis, was prepared *via* the facile co-precipitation method using a versatile double-hydrophilic block copolymer comprising of a DS segment (ligand for SR-A) and a poly(glyclerol methacrylate) segment (SPIONs surface-anchoring unit). The physicochemical properties of the DS-SPIONs were investigated using various instruments. DS-SPIONs exhibited high aqueous stability compared to dextran-coated SPIONs (Dex-SPIONs), which were used as controls. The cellular uptake behaviors of DS-SPIONs and Dex-SPIONs were evaluated using Prussian blue assay. Interestingly, the DS-SPIONs were effectively taken up by activated macrophages compared to Dex-SPIONs. However, the cellular uptake of DS-SPIONs by activated macrophages was remarkably reduced in the presence of free DS. These results suggest that activated macrophages internalize DS-SPIONs *via* receptor (SR-A)-mediated endocytosis. T_2-weighted MR imaging of the cells demonstrated that activated macrophages treated with DS-SPIONs showed a significantly lower signal intensity compared to those treated with Dex-SPIONs. Overall, these results suggest that DS-SPIONs may be utilized as a potential contrast agent for atherosclerosis MR imaging.

1. Introduction

Atherosclerotic vascular disease remains the leading cause of morbidity and mortality worldwide (Fonarow, 2007). The high mortality of atherosclerosis is primarily due to the unavailability of effective tools that diagnose the disease early in its pathogenesis. Atherosclerosis is an inflammatory disease that is characterized by a build-up of lipid-rich plaques within arterial walls, which eventually lead to life-threatening clinical conditions such as myocardial infractions and strokes (Libby, Ridker & Maseri, 2002; Libby, 2002; Ross, 1999). The conventional diagnostic methods for atherosclerosis mainly assess plaque burden and are often inaccurate and too invasive. Specifically, coronary angiography is the most common procedure to detect atherosclerosis, but is capable of only detecting stenosis and provides no information that would differentiate vulnerable from unstable plaques (MacNeill, Lowe, Takano, Fuster & Jang, 2003). Vulnerable plaques are more dangerous because they do not reveal any symptom or clinical sign before a sudden rupture resulting in arterial occlusion (Falk, 2006). Therefore, assessment of functional changes during the early stage of atherosclerosis is essential for prognosis and its clinical management.

The advent of new imaging modalities has opened new avenues in visualizing and characterizing biological processes at the cellular and molecular levels. In recent years, magnetic resonance (MR) imaging has garnered enormous attention due to its ability to provide anatomical and functional assessments of blood vessels in a non-invasive, reliable and safe manner without exposure to ionizing irradiation (Briley-Saebo et al., 2007; Phinikaridou et al., 2010; Sosnovik, Nahrendorf & Weissleder, 2007). However, MR imaging requires a contrast-enhancing agent for effective detection and characterization of plaque composition or molecular events of the disease at the cellular level. For decades, gadolinium chelates and iron oxide nanoparticles have been widely employed as contrast agents for *in vivo* MR imaging (Barkhausen, Ebert, Heyer, Debatin &

* Corresponding author at: Departments of Polymer Science and Chemical Engineering, College of Engineering, Sungkyunkwan University, Suwon 440-746, Republic of Korea. Tel.: +82 31 290 7288; fax: +82 31 292 8790.
E-mail addresses: jhpark1@skku.edu, biopol@gmail.com (J.H. Park).
[1] These authors contributed equally to this paper.

0144-8617/$ – see front matter © 2013 Elsevier Ltd. All rights reserved.
http://dx.doi.org/10.1016/j.carbpol.2013.10.068

Weinmann, 2003; Waters & Wickline, 2008). However, since most of their molecular targets are expressed at very low concentrations, high concentrations of these contrast agents are required for signal enhancement in these imaging techniques (Choudhury, Fuster & Fayad, 2004; Gallino et al., 2012; Wickline, Neubauer, Winter, Caruthers & Lanza, 2007). In this regard, the use of iron oxide nanoparticle-based contrast agents is highly advantageous due to the following reasons: (1) each nanoparticle possesses thousands of iron atoms that dramatically enhance sensitivity; (2) the surface of the nanoparticle can be tailor-made with specific ligands to improve targeting efficiency; and (3) nanoparticles can be engineered as multimodal imaging agents (Kelly et al., 2005; McCarthy, 2010; Saravanakumar, Kim, Park, Rhee & Kwon, 2009). Currently, dextran-coated superparamagentic iron oxide nanoparticles (Dex-SPIONs) are clinically available as MR imaging contrast agents for the diagnosis of various disease (Tassa, Shaw & Weissleder, 2011).

The formation of atherosclerotic plaques involves a number of sequential events and activated macrophages play an essential role in all phases from the development of the fatty streak to plaque rupture (Li & Glass, 2002; Libby, DiCarli & Weissleder, 2010). Therefore, efficient internalization of a contrast agent by activated macrophages may allow for the identification of progression of the disease using MR imaging before luminal narrowing. Although Dex-SPIONs have shown the potential to detect atherosclerotic plaque, the uptake process by activated macrophages is non-specific and the contrast enhancement produced is not sufficient to discern the plaque/lumen boundaries (Kooi et al., 2003; Sadat, Li, Graves, Tang & Gillard, 2009; Trivedi et al., 2004). The targetability of SPIONs can be improved by conjugating specific ligands for macrophages to the surface of nanoparticles. In the early atherosclerotic process, macrophages substantially over-express scavenger receptors that bind and internalize oxidized low-density lipoprotein, maleylated or glycated bovine serum albumin and polyanionic macromolecules (Li & Glass, 2002). Dextran sulfate (DS), a polyanionic derivative of dextran, acts as a ligand for surface receptor class A (SR-A) – a receptor over-expressed on activated macrophages in the atherosclerotic region but not expressed on endothelial cells in normal aortic vessels (de Winther, van Dijk, Havekes, & Hofker, 2000; Linton & Fazio, 2001). Consequently, a target-specific contrast agent for imaging atherosclerotic macrophages may be fabricated by coating the SPIONs with DS. However, the conventional co-precipitation method, which is employed for the preparation of Dex-SPIONs, cannot be exploited to produce DS-coated SPIONs (DS-SPIONs). In recent years, efforts have been made to decorate the surface of SPIONs with DS. Specifically, a small amount of DS was added into solution during the preparation of Dex-SPIONs by the co-precipitation method (Benjamin, Michele, Jacob & Angelique, 2007). In addition, sulfonation of Dex-SPIONs was carried out in order to mimic characteristics of DS-SPIONs (Tu et al., 2011). However, these methods were unable to guarantee complete, stable decoration of SPIONs with the DS.

In an attempt to address this issue, we have designed a tailor-made double hydrophilic DS-*b*-poly(glycerol methacrylate) (DS-b-PGMA) copolymer, composed of a DS segment as a ligand for SR-A on an activated macrophage and a PGMA segment as the surface-anchoring unit for SPIONs. By utilizing the DS-*b*-PGMA copolymer, DS-SPIONs were readily prepared using a simple co-precipitation method. The physicochemical characteristics such as size, stability and magnetic properties of DS-SPIONs were investigated. In addition, the *in vitro* cellular uptake behavior of DS-SPIONs by activated macrophages and their potential as the MR imaging agent for diagnosis of atherosclerosis were explored.

2. Materials and methods

2.1. Materials

Dextran sulfate sodium (Mw = 4000) was purchased from TCI chemical (Tokyo, Japan). Glycerol monomethacrylate (GMA) was obtained from Polysciences Inc. (Warrington, PA, USA). Iron (III) chloride hexahydrate ($FeCl_3{\cdot}6H_2O$, 97%), iron (II) chloride tetrahydrate ($FeCl_2{\cdot}4H_2O$, 99%), sodium hydroxide (NaOH), sodium cyanoborohydride ($NaCNBH_3$), 2-aminoethanethiol hydrochloride (AET·HCl), 2,2′-azobisisobutyronitrile (AIBN), and anhydrous *N*,*N*-dimethylformamide (DMF) were purchased from Sigma–Aldrich (St. Louis, MO, USA). AIBN was used following purification by recrystallization in methanol. Water used in all the experiments was purified using the AquaMax-Ultra water purification system (Yonglin Co., Anyang, Korea). All other chemicals were obtained from commercial sources and used as received.

2.2. Synthesis of amine-terminated PGMA (PGMA-NH_2)

PGMA-NH_2 was synthesized by free radical polymerization of GMA in the presence of AET·HCl and AIBN as the chain transfer agent and initiator, respectively. In a typical reaction, GMA (3 g, 25.82 mmol), AET·HCl (146.67 mg, 1.29 mmol) and AIBN (21.21 mg, 0.13 mmol) were dissolved in 18 ml of DMF in a Schlenk flask. The mixture was subjected to three freeze–pump–thaw cycles and the flask was immersed in a preheated oil bath maintained at 60 °C. After 12 h, PGMA-NH_2 was obtained by precipitation in excess of diethyl ether, followed by drying under vacuum at room temperature.

2.3. Synthesis of DS-b-PGMA copolymer

DS-b-PGMA was synthesized by the reaction of DS with PGMA-NH_2 in the presence of $NaCNBH_3$ as the reducing agent according to the general experimental procedure for reductive amination (Schatz, Louguet, Le Meins, & Lecommandoux, 2009). In brief, DS (332 mg) was dissolved in acetate buffer (50 mM, pH 5.0) at 50 °C. After addition of PGMA-NH_2 (200 mg) and $NaCNBH_3$ (130.4 mg) to the solution, the mixture was stirred at 50 °C for 96 h with a daily addition of 25 equivalent of $NaCNBH_3$ based on the amount of DS. The resulting solution was dialyzed for 4 days against deionized water, followed by lyophilization in order to obtain the copolymer as a white powder.

2.4. Preparation of DS-SPIONs

DS-SPIONs were prepared by coating the SPIONs surface with DS-*b*-PGMA copolymer *via* a facile co-precipitation method (Lee et al., 2011). In a typical procedure, $FeCl_3{\cdot}6H_2O$ (1.014 g) and $FeCl_2{\cdot}4H_2O$ (0.36 g) were dissolved in deoxygenated distilled water (18.75 ml). Subsequently, 3 M NaOH (7.5 ml) was added to the solution in a dropwise manner at 80 °C under nitrogen atmosphere. The formation of SPIONs was noticed with a change in color to dark black. Subsequently, DS-*b*-PGMA copolymer (412.2 mg) was added to the solution. Stirring was continued for an additional 1 h. Subsequently, the particles were separated by centrifugation and washed three times with deoxygenated water to remove the unwanted ions and excess of copolymer. The resulting DS-SPIONs were stored at 4 °C, prior to use. As the control, Dex-SPIONs were prepared in an identical manner.

2.5. Characterization

^{1}H NMR spectra were recorded on a JEOL JNM-AL300 (300 MHz) spectrometer (Tokyo, Japan) from samples that were dissolved

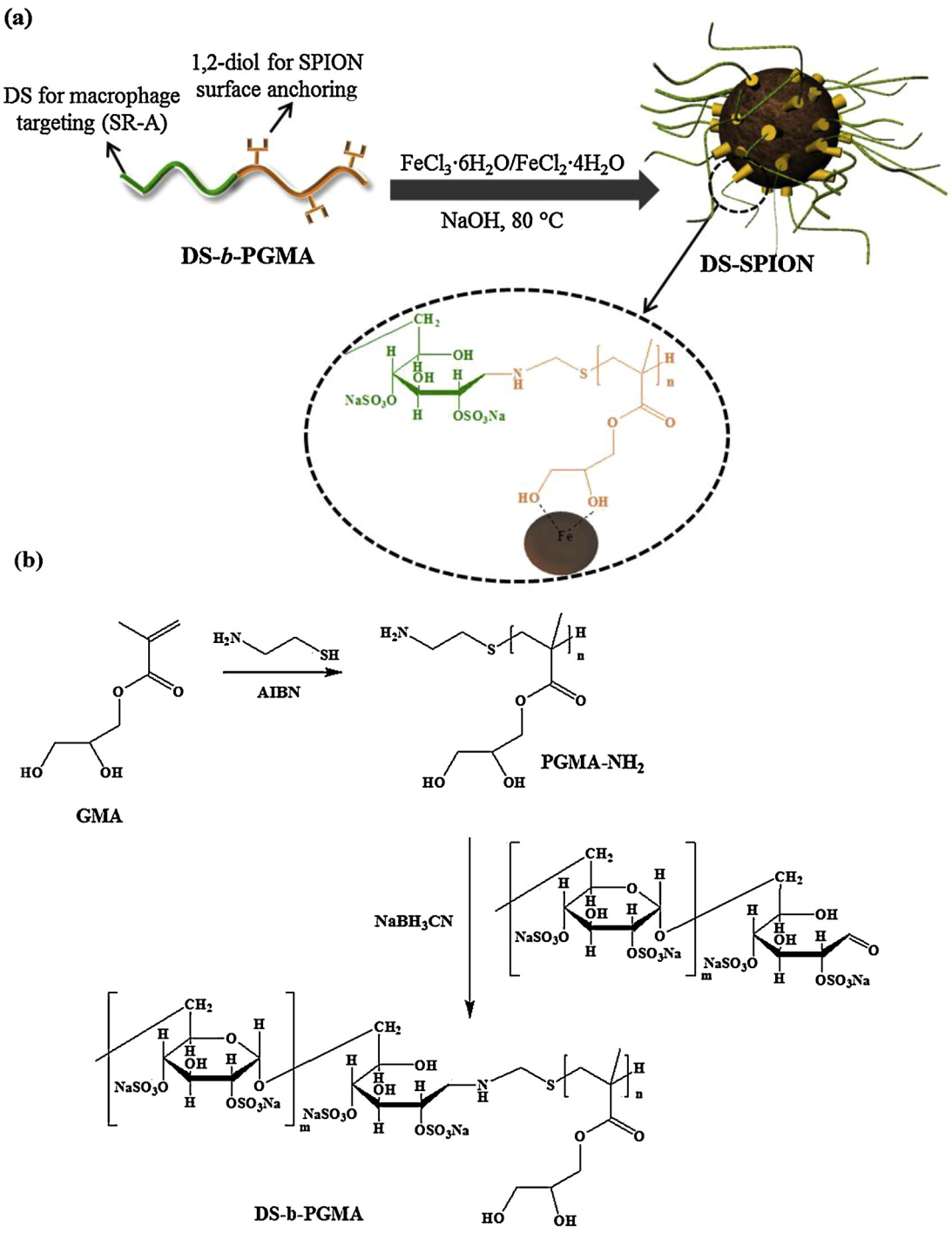

Fig. 1. (a) Illustration of interactions between 1,2-diols of DS-*b*-PGMA and the SPION iron atom and (b) reaction scheme for synthesis of DS-*b*-PGMA copolymer.

in D_2O. Fourier transform infrared (FT-IR) spectra were obtained using a Bruker IFS-66v FT-IR spectrometer (Germany). The dried samples were ground with KBr powder and the mixture was made into pellets. The spectra were recorded in the range of 400–4000 cm^{-1} with a resolution of 4 cm^{-1}. Thermogravimetric analysis (TGA) was performed under the flow of nitrogen gas at an outlet pressure of 6–10 kg/cm^2 with a heating rate of 20 °C/min from 20 to 600 °C. Transmission electron microscope (TEM) images were taken on a JEM-2100F (JEOL, Tokyo, Japan) operating at an accelerating voltage of 200 kV. The samples were prepared by depositing nanoparticular suspensions onto a carbon-coated copper grid (200 mesh). The average hydrodynamic size and distribution of the nanoparticles were determined using dynamic light scattering (DLS, FPAR-1000, Otsuka Electronics, Osaka, Japan). The stability of the nanoparticles was investigated by dispersing the nanoparticles in a phosphate-buffered saline (PBS pH 7.4) and measuring the change in hydrodynamic size of the particles as a function of time at 37 °C.

2.6. In vitro cellular uptake tests

Macrophages (RAW264.7) and bovine aortic endothelial cells (BAEC) were purchased from the American Type Culture Collection (Rochkville, MD, USA). Bare RAW264.7 and activated RAW264.7

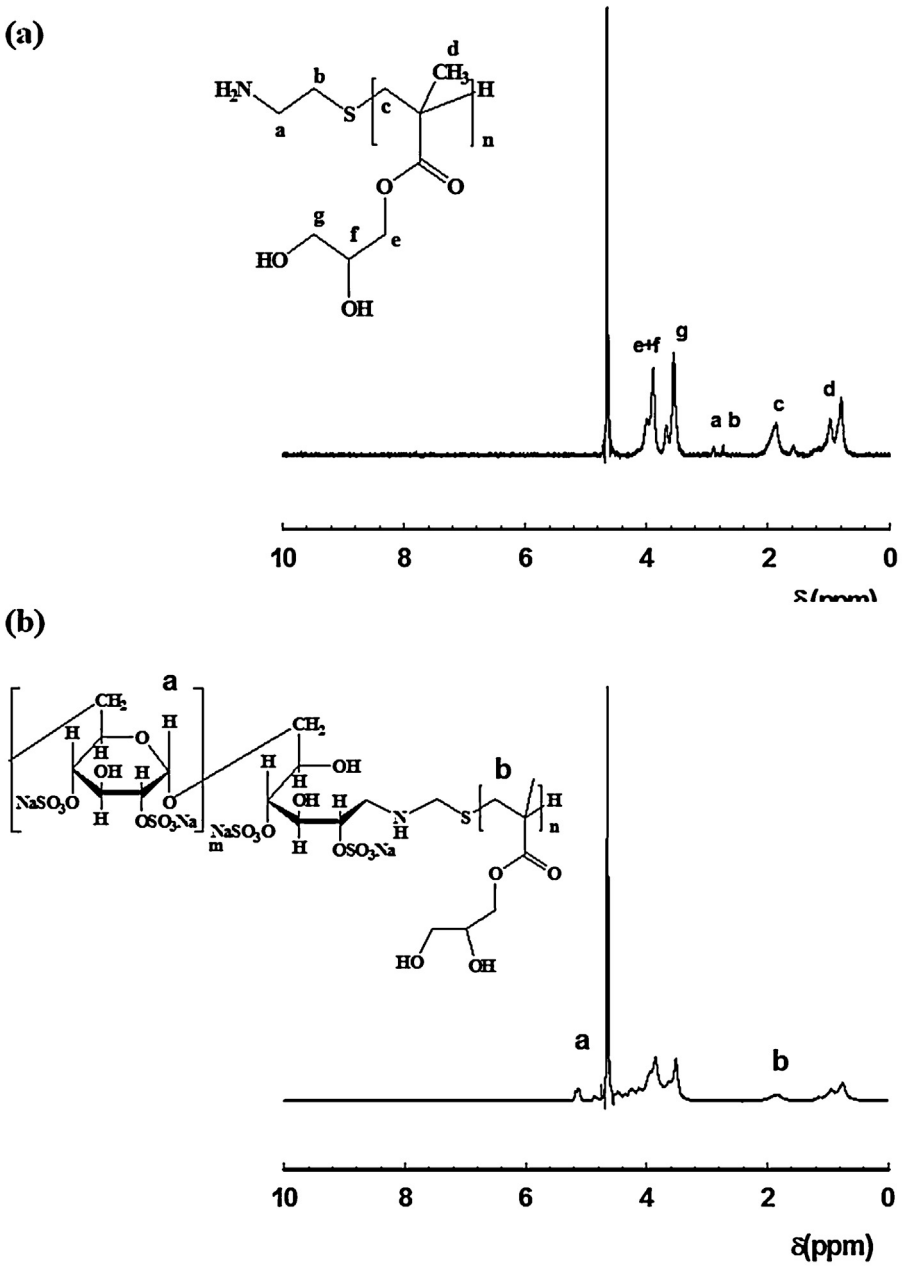

Fig. 2. ^{1}H NMR spectra of (a) PGMA-NH_2 and (b) DS-*b*-PGMA.

were plated at 2×10^5 cells/ml and maintained in media (RPMI-1640 with 10% FBS and 1% antibiotic–antimycotic solution) at 37 °C in a 5% CO_2 atmosphere overnight which allowed cells to adhere to the dishes. The bare macrophages were activated by treating them with lipopolysaccharide (LPS, 20 ng/ml) (Shen et al., 2008). BAEC were plated at 2×10^5 cells/ml and maintained in media (low glucose DMEM with 20% FBS and 1% antibiotic–antimycotic solution) at 37 °C in a 5% CO_2 atmosphere overnight which allowed cells to adhere to the dishes. Following the removal of media, DS-SPIONs or Dex-SPIONs ([Fe] = 25 μg/ml) solution was introduced to the cells and incubated at 37 °C in 5% CO_2 atmosphere for 30 min. Subsequently, the cells were stained according to the Prussian blue assay protocol. A competitive inhibition study was utilized in order to determine the cellular uptake of DS-SPIONs. The medium was replaced with free DS (5 mg/ml) and DS-SPIONs ([Fe] = 25 μg/ml) in activated RAW264.7, followed by an incubation at 37 °C in 5% CO_2 atmosphere for 30 min. The cells were stained in an identical manner. The intracellular localizations of DS-SPIONs and Dex-SPIONs were observed using an OLYMPUS BX51 microscope (Tokyo, Japan).

2.7. MRI relaxation properties

MR relaxivity of the DS-SPIONs was measured using an animal 4.7 T Bruker Biospin Imager (Bruker Medical Systems, Karlsruhe, Germany). Each sample was dissolved into distilled water ([Fe] = 0.25, 0.125, 0.063, 0.031, 0.016, 0.008 mM). The imaging parameters were as follows: TR, 2000 ms; TE, 10.149 ms; slice thickness, 1.5 mm; field of view (FOV), 81.323 mm × 50 mm; and matrix size; 256 × 192.

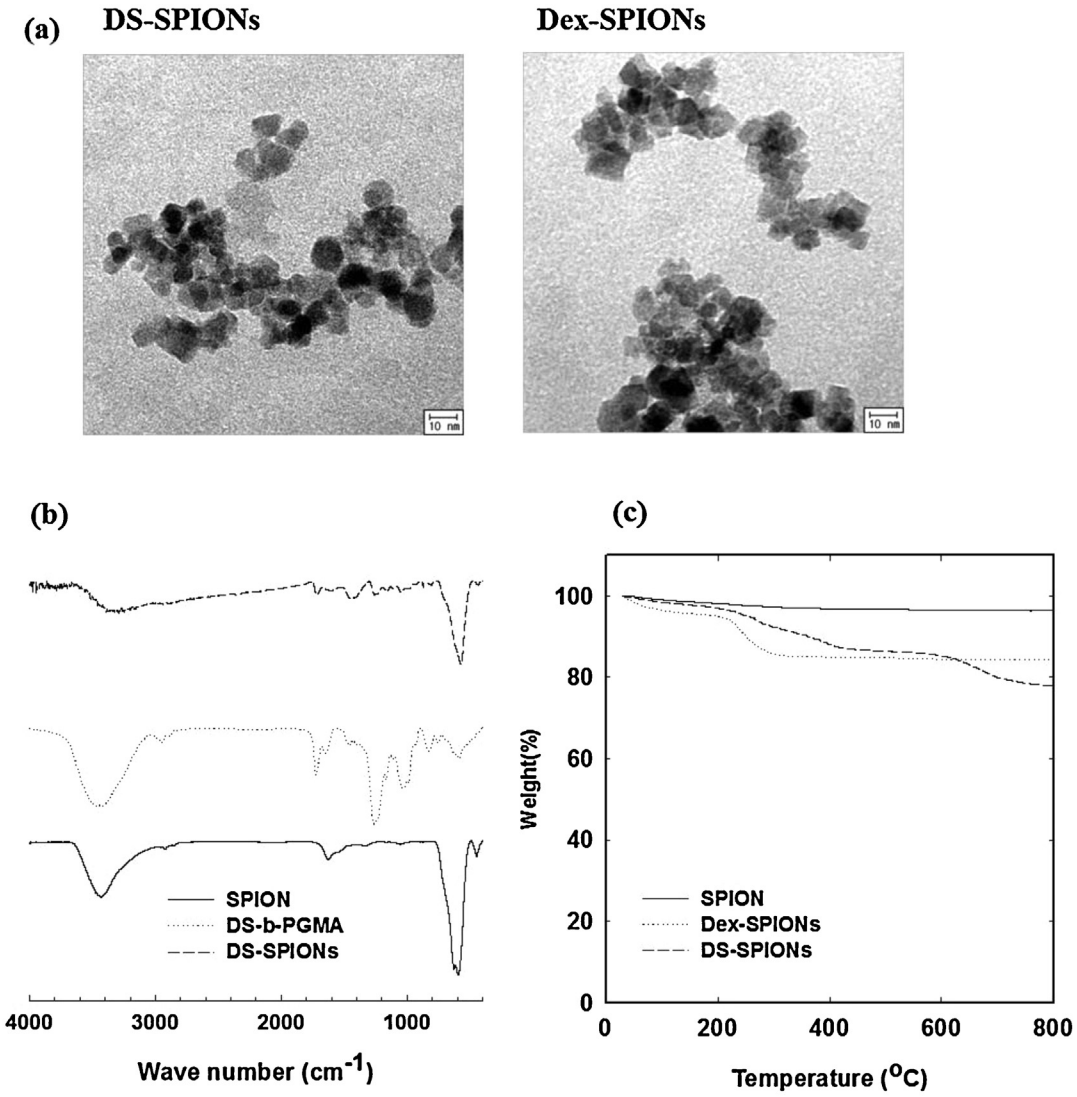

Fig. 3. The characteristics of superparamagnetic nanoparticles: (a) TEM images, (b) FT-IR spectra and (C) TGA curves.

2.8. In vitro MR imaging

The cellular uptake of the nanoparticles was carried out in an identical manner as described earlier. After the cells were treated with DS-SPIONs and Dex-SPIONs for 30 min, the cells were washed twice with PBS. Following centrifugation, the media containing 6×10^8 cells/ml was transferred to a 1.5 ml test tube. Cell pellets were obtained by placing the tube in an undisturbed setting for 3 h. T_2-weighted MR images of cell pellets were obtained with a head coil on a 4.7 T MR scanner. The imaging parameters were as follows: TR, 468.575 ms; TE, 10.407 ms; slice thickness, 1.0 mm; field of view (FOV), 40 mm × 40 mm; matrix size; 256 × 256.

3. Results and discussion

MR imaging has shown great promise for assessing molecular and cellular components of atherosclerotic plaques due to its high resolution and signal-to-noise ratio (Amirbekian et al., 2007). Macrophages play a prominent role in the formation, progression and the destabilization of the atherosclerotic plaque (Choudhury, Lee & Greaves, 2005). The development of activated macrophage-targeted contrast enhancing agents may greatly improve the accuracy and detection limit of MR imaging for atherosclerosis. In this respect, DS-SPIONs may have potential as an MR contrast agent because of their ability to be selectively incorporated into activated macrophages *via* SR-A-mediated endocytosis.

3.1. Synthesis and characterization of DS-b-PGMA copolymer

In order to prepare DS-SPIONs, a new double hydrophilic DS-*b*-PGMA copolymer comprising a DS segment as a ligand for activated macrophages and a PGMA segment containing 1,2-diol moieties for the robust attachment on the surface of SPIONs (Fig. 1a) was synthesized. The synthetic strategy for the preparation of the DS-*b*-PGMA block copolymer is shown in Fig. 1b. First, PGMA-NH_2 was synthesized by radical polymerization of GMA using AET·HCl as a chain transfer agent and AIBN as the initiator. The chemical structure of PGMA-NH_2 was confirmed using ^{1}H NMR spectrum (Fig. 2a). The average molecular weight of PGMA-NH_2 was 3800 Da which was determined by comparing the peak integration values from the GMA moiety (—CH_2—CH(OH)—) at 3.89–3.98 ppm and the AET moiety of the polymeric chain end (—S—CH_2—CH_2—NH_2) at 2.89 ppm. Polysaccharide-based diblock copolymers were synthesized by the chemical reaction between the aldehyde group at the chain end of the polysaccharide and an amine-functionalized homopolymer (Schatz & Lecommandoux, 2010; Schatz et al., 2009). In this study, DS-*b*-PGMA was readily synthesized by reacting DS with PGMA-NH_2 *via* conventional reductive amination in the

presence of sodium cyanoborohydride. The successful formation of the block copolymer was confirmed by the ^{1}H NMR spectrum of DS-*b*-PGMA (Fig. 2b), which exhibited the characteristic peaks for the anomeric proton of DS at 5.13 ppm (Yang & Zhang, 2009) and for the methylene group of PGMA at 1.82 ppm.

3.2. Preparation and characterization of DS-SPIONs

By employing DS-*b*-PGMA which has the ability to form a stable 5-membered chelate ring with the iron oxide surface through cis-1,2-diols of the PGMA block, DS-SPIONs were readily prepared using the facile co-precipitation process. Dex-SPION was also prepared as a control by the same procedure in which hydroxyl groups in Dex were considered to form weak coordinating groups for SPIONs (Zhang, Wang, Qiao, Yan & Liu, 2009). The average hydrodynamic size of DS-SPIONs was measured using a DLS and was 64 ± 5.65 nm which was comparable to that of Dex-SPIONs (65 ± 11.20 nm). The hydrodynamic size distribution of DS-SPIONs and Dex-SPIONs was fairly monodisperse (Supporting Information Fig. S1). The particle size and morphology of the nanoparticles were evaluated using TEM. As shown in Fig. 3a, although the particles aggregated during sample preparation under the dried condition, the average particle sizes of both DS-SPIONs and Dex-SPIONs may be smaller than those determined using DLS. This discrepancy is attributed to the fact that DLS provides the mean size of the magnetic core along with the surrounding hydrodynamic polymer layer whereas the TEM image shows the inorganic particle core alone (Lee et al., 2006). The morphology of all the nanoparticles as observed through TEM revealed the coexistence of spherical, non-spherical and ellipsoidal particles.

Supplementary material related to this article can be found, in the online version, at http://dx.doi.org/10.1016/j.carbpol.2013.10.068.

FT-IR spectra of DS-SPIONs, DS-*b*-PGMA and bare SPIONs are shown in Fig. 3b. The presence of characteristic peaks for ester carbonyl groups of PGMA block at 1722 cm^{-1}, asymmetric stretching vibration of sulfate group from DS at 1261 cm^{-1} and Fe-O stretching vibration at 575 cm^{-1} in the DS-SPIONs confirmed the successful coating of block copolymers on the surface of nanoparticles (Lee et al., 2011; Tu, Ma, Pantazis, Kauzlarich & Louie, 2010). The TGA curves for DS-SPIONs, Dex-SPIONs and bare SPIONs are shown in Fig. 3c. The bare SPIONs exhibited a weight loss of 1.89% between temperatures ranging from 25 °C to 200 °C resulting from the bound or surface-adsorbed water molecules on the nanoparticles (Lee et al., 2011). No appreciable weight loss was noted up to 800 °C. In contrast, DS-SPIONs and Dex-SPIONs showed significant weight loss above 200 °C indicating the degradation of coated polymers. Dex-SPIONs exhibited a one-step weight loss above 200 °C whereas DS-SPIONs underwent a two-step thermal degradation process. The first weight loss of DS-SPIONs between 200 and 450 °C could be attributed to the degradation of DS and some portions of the PGMA segment that were not bound to the inorganic particle core. The second weight loss over the temperature range of 550 °C could be due to degradation of the PGMA segment that was chemisorbed on the surface of the particle core. This degradation behavior of the PGMA was also noted by Zhang, Wang, Qiao, Yan and Liu (2009) who demonstrated that the PGA segment bound to the SPIONs requires higher temperatures for degradation. Amounts of polymers coated on the surface of the SPIONs were found to be 20.18 and 13.73 wt% for DS-SPIONs and Dex-SPIONs, respectively. This indicates that, owing to the high binding affinity of the PGMA segment to SPIONs, the amount of DS-*b*-PGMA on the SPIONs was relatively higher than that of Dex.

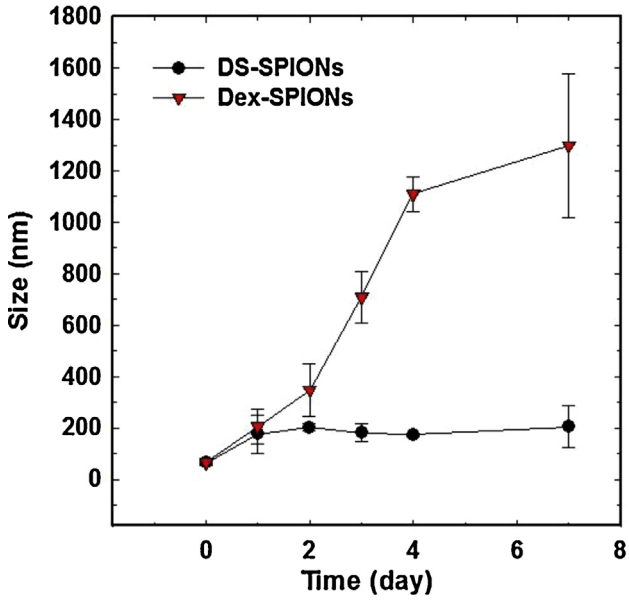

Fig. 4. Particle size of nanoparticles in PBS (pH 7.4) as a function of time. The error bar represents the standard deviation ($n = 3$).

3.3. Stability and magnetic property of nanoparticles

The stability of the nanoparticles is a highly important parameter for successful biomedical applications. If the surface-coated polymer layer is not robust, the nanoparticles may tend to agglomerate and precipitate under aqueous conditions (Amstad, Textor & Reimhult, 2011; Di Marco et al., 2007). The stability of DS-SPIONs and Dex-SPIONs in PBS (pH 7.4) was investigated by measuring

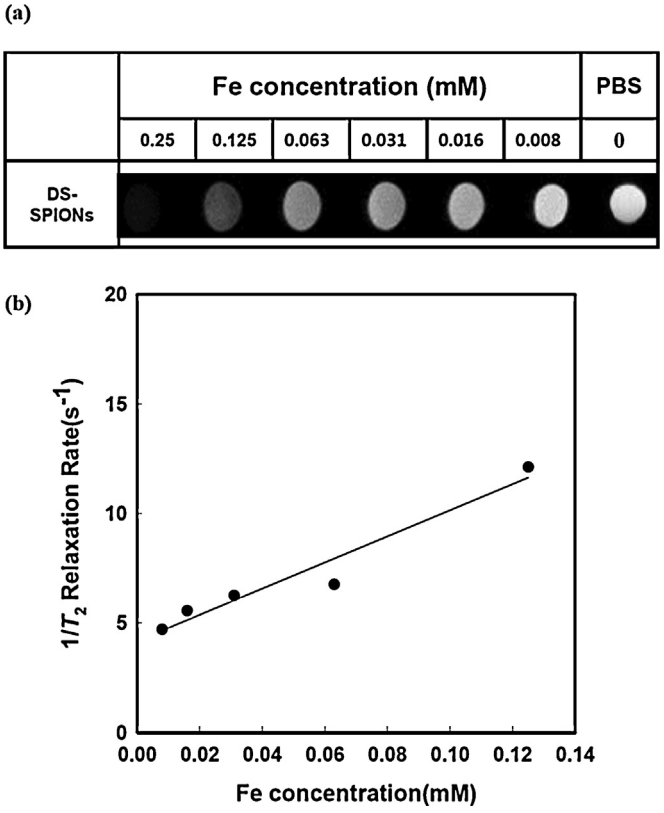

Fig. 5. (a) T_2-weighted images of DS-SPIONs at various iron concentrations, (b) T_2 relaxation rate ($1/T_2$) as a function of iron concentration for DS-SPIONs.

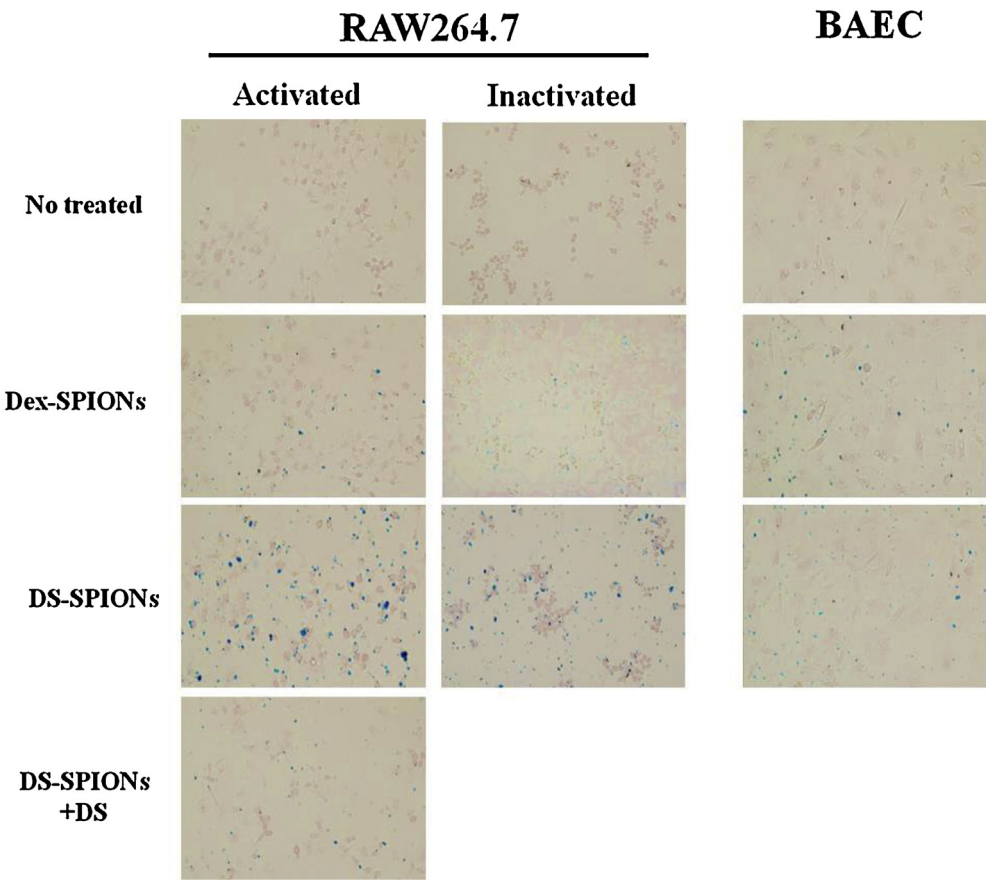

Fig. 6. Microscopic images of LPS-activated RAW264.7, inactivated RAW264.7 and BAEC cells. The cells were stained by Prussian blue assay following treatment with nanoparticles.

their change in hydrodynamic size as a function of time at 37 °C. As shown in Fig. 4, Dex-SPIONs rapidly aggregated to form large particles (≥1000 nm) within 3 days whereas DS-SPIONs were relatively stable with a slight increase in size for up to 7 days. The poor stability of Dex-SPIONs might be due to desorption of Dex from the nanoparticles followed by their aggregation (Paul, Frigo, Groman & Groman, 2004). The bare SPIONs were highly unstable and precipitated by aggregation within one day post-incubation (data not shown). These results suggest that compared to bare SPIONs and Dex-SPIONs, DS-SPIONs have higher stability, which is primarily ascribed to the presence of a robust and hydrophilic DS-*b*-PGMA layer. This is in agreement with previous studies which investigated the stability of magnetic nanoparticles coated with polymers bearing 1, 2-diols (Hu, Qian, Wang, Liu & Liu, 2011; Wan, Huang, Yan & Liu, 2006; Wan, Zheng, Liu, Yan & Liu, 2005). *In vivo* biodistribution and clearance of SPIONs are greatly influenced by their physicochemical properties such as size and surface characteristics (Jain, Reddy, Morales, Leslie-Pelecky & Labhasetwar, 2008; Yoon et al., 2012). Given the small particle size and high stability of DS-SPIONs with the hydrophilic surface, DS-SPIONs are expected to show prolonged circulation in blood, which may increase their possibility to reach the target site and allow enhanced MR imaging.

In order to observe the contrast effect of DS-SPIONs, T_2-weighted MR images were obtained from the nanoparticular dispersions at various concentrations. As shown in Fig. 5a, darkness of DS-SPIONs on T_2-weighed images increased in a Fe concentration-dependent manner. The T_2 relaxivity (r_2, $mM^{-1}\,s^{-1}$) of DS-SPIONs was calculated from the slope of the graph for $1/T_2$ *vs.* the Fe concentration (Fig. 5b), which showed an r_2 value of 59.62 $mM^{-1}\,s^{-1}$. These results indicate that DS-SPIONs could be used as a potential contrast agent for MR imaging.

3.4. *In vitro* cellular uptake

The cellular uptake behavior of DS-SPIONs and Dex-SPIONs was investigated using RAW264.7 murine macrophage cells. Several studies have shown that RAW264.7 is activated by LPS resulting in the over-expression of SR-A (Fitzgerald, Moore, Freeman & Reed, 2000). In order to demonstrate the receptor (SR-A)-mediated cellular uptake of DS-SPIONs, nanoparticles were incubated with activated RAW264.7, inactivated RAW264.7 and BAEC that does not over-express the SR-A. Following 30 min of incubation, the uptake of nanoparticles was confirmed using the Prussian blue staining assay. As shown in Fig. 6, blue color was detected in the activated and inactivated RAW264.7 cells incubated with DS-SPIONs. Interestingly, activated cells showed more prominent blue spots than the inactivated cells suggesting that up-regulation of SR-A in the activated cells facilitated uptake of DS-SPIONs. In contrast, Dex-SPIONs, which were used as controls, demonstrated no binding ability to the SR-A and showed poor uptake by both activated and inactivated RAW264.7 cells. All nanoparticles were rarely taken up by the BAEC without SR-A. These results indicate that DS-SPIONs were incorporated into cells through SR-A-mediated endocytosis. In order to further substantiate this assumption, a competition inhibition study was performed by pre-incubating cells with a high dose of free DS prior to DS-SPIONs treatment. Incubation with free DS dramatically reduced the cellular uptake of DS-SPIONs. These results clearly suggest that DS-SPIONs selectively bind to the SR-A

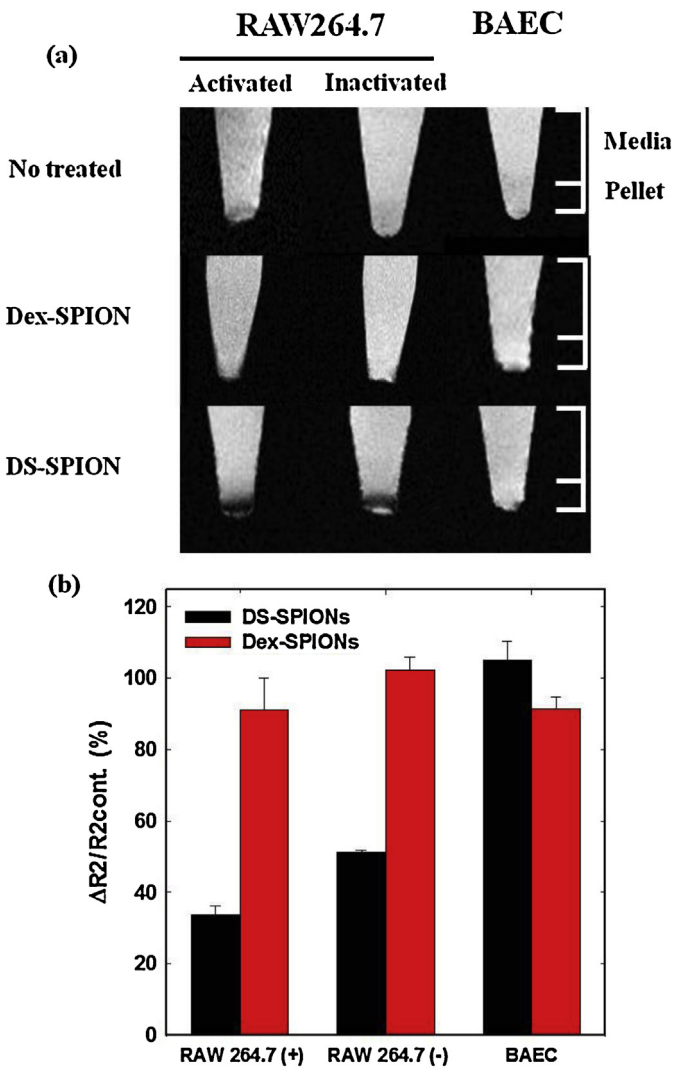

Fig. 7. (a) T_2-weighted MR images and (b) relative signal intensity of RAW264.7 and BAE cells after incubation with nanoparticles. The error bar represents the standard deviation ($n = 3$).

of macrophages and are subsequently internalized *via* receptor-mediated endocytosis.

3.5. In vitro cellular imaging

To investigate the potential of DS-SPIONs as a target-specific contrast agent, T_2-weighted MR cell imaging was performed using activated RAW264.7, inactivated RAW264.7 and BAEC (Fig. 7). The highest MR contrast effect was observed for activated RAW264.7 treated with DS-SPIONs. In contrast, Dex-SPIONs showed negligible contrast effects for both activated and inactivated RAW264.7 cells. Furthermore, no significant MR contrast enhancements were noted for BAECs treated with both DS-SPIONs and Dex-SPIONs (Fig. 7a). These results corroborate the findings from the Prussian blue assay supporting receptor-mediated endocytosis of DS-SPIONs. We also quantitatively determined the relative MR signal intensities for the cells treated with DS-SPIONs and Dex-SPIONs compared to the untreated cells (Fig. 7b). For Dex-SPIONs, no significant changes in the intensities were found for both activated and inactivated RAW264.7. The relative intensities for DS-SPION-treated activated and inactivated RAW264.7 cells decreased remarkably and were $33 \pm 1.41\%$ and $51.34 \pm 0.26\%$, respectively. This result also supports receptor-mediated endocytosis of DS-SPIONs. Taken together, these findings suggest that DS-SPIONs could be utilized as a target-specific MR contrast agent for atherosclerosis imaging.

4. Conclusion

In summary, we have prepared DS-SPIONs *via* the facile co-precipitation method by employing a novel double-hydrophilic DS-b-PGMA block copolymer and utilized DS-SPIONs as a potential contrast agent for atherosclerosis MR imaging. DS-SPIONs showed excellent stability compared to Dex-SPIONs primarily due to the robust anchoring of DS-*b*-PGMA on the surface of SPIONs through the formation of five-membered chelating rings between 1,2-diols of the PGMA segment and the SPIONs. In particular, DS-SPIONs were specifically taken up by the activated macrophages *via* receptor-mediated endocytosis and produced distinct contrast enhancement in the T_2-weighted MR cellular imaging of activated macrophages. Overall, these results suggest that DS-SPIONs have the potential to be utilized as targeted MR contrast agents for atherosclerosis imaging.

Acknowledgements

This work was financially supported by the Basic Science Research Programs (20100027955 & 2012012827) of MEST.

References

Amirbekian, V., Lipinski, M. J., Briley-Saebo, K. C., Amirbekian, S., Aguinaldo, J. G. S., Weinreb, D. B., et al. (2007). Detecting and assessing macrophages in vivo to evaluate atherosclerosis noninvasively using molecular mri. *Proceedings of the National Academy of Sciences*, *104*(3), 961–966.

Amstad, E., Textor, M., & Reimhult, E. (2011). Stabilization and functionalization of iron oxide nanoparticles for biomedical applications. *Nanoscale*, *3*(7), 2819–2843.

Barkhausen, J., Ebert, W., Heyer, C., Debatin, J. F., & Weinmann, H.-J. (2003). Detection of atherosclerotic plaque with gadofluorine-enhanced magnetic resonance imaging. *Circulation*, *108*(5), 605–609.

Benjamin, R. J., Michele, F., Jacob, V., & Angelique, Y. L. (2007). Size-controlled synthesis of dextran sulfate coated iron oxide nanoparticles for magnetic resonance imaging. *Nanotechnology*, *18*(3), 035603.

Briley-Saebo, K. C., Mulder, W. J. M., Mani, V., Hyafil, F., Amirbekian, V., Aguinaldo, J. G. S., et al. (2007). Magnetic resonance imaging of vulnerable atherosclerotic plaques: Current imaging strategies and molecular imaging probes. *Journal of Magnetic Resonance Imaging*, *26*(3), 460–479.

Choudhury, R. P., Fuster, V., & Fayad, Z. A. (2004). Molecular, cellular and functional imaging of atherothrombosis. *Nature Reviews Drug Discovery*, *3*(11), 913–925.

Choudhury, R. P., Lee, J. M., & Greaves, D. R. (2005). Mechanisms of disease: Macrophage-derived foam cells emerging as therapeutic targets in atherosclerosis. *Nature Clinical Practice Cardiovascular Medicine*, *2*(6), 309–315.

de Winther, M. P. J., van Dijk, K. W., Havekes, L. M., & Hofker, M. H. (2000). Macrophage scavenger receptor class a. *Arteriosclerosis. Thrombosis, and Vascular Biology*, *20*(2), 290–297.

Di Marco, M., Sadun, C., Port, M., Guilbert, I., Couvreur, P., & Dubernet, C. (2007). Physicochemical characterization of ultrasmall superparamagnetic iron oxide particles (uspio) for biomedical application as mri contrast agents. *International Journal of Nanomedicine*, *2*(4), 609–622.

Falk, E. (2006). Pathogenesis of atherosclerosis. *Journal of the American College of Cardiology*, *47*(8 Suppl.), C7–C12.

Fitzgerald, M. L., Moore, K. J., Freeman, M. W., & Reed, G. L. (2000). Lipopolysaccharide induces scavenger receptor a expression in mouse macrophages: A divergent response relative to human thp-1 monocyte/macrophages. *Journal of Immunology*, *164*(5), 2692–2700.

Fonarow, G. C. (2007). The global burden of atherosclerotic vascular disease. *Nature Clinical Practice Cardiovascular Medicine*, *4*(10), 530–531.

Gallino, A., Stuber, M., Crea, F., Falk, E., Corti, R., Lekakis, J., et al. (2012). In vivo imaging of atherosclerosis. *Atherosclerosis*, *224*(1), 25–36.

Hu, J., Qian, Y., Wang, X., Liu, T., & Liu, S. (2011). Drug-loaded and superparamagnetic iron oxide nanoparticle surface-embedded amphiphilic block copolymer micelles for integrated chemotherapeutic drug delivery and mr imaging. *Langmuir*, *28*(4), 2073–2082.

Jain, T. K., Reddy, M. K., Morales, M. A., Leslie-Pelecky, D. L., & Labhasetwar, V. (2008). Biodistribution, clearance, and biocompatibility of iron oxide magnetic nanoparticles in rats. *Molecular Pharmaceutics*, *5*(2), 316–327.

Kelly, K. A., Allport, J. R., Tsourkas, A., Shinde-Patil, V. R., Josephson, L., & Weissleder, R. (2005). Detection of vascular adhesion molecule-1 expression using a novel multimodal nanoparticle. *Circulation Research*, *96*(3), 327–336.

Kooi, M. E., Cappendijk, V. C., Cleutjens, K. B. J. M., Kessels, A. G. H., Kitslaar, P. J. E. H. M., Borgers, M., et al. (2003). Accumulation of ultrasmall superparamagnetic

particles of iron oxide in human atherosclerotic plaques can be detected by in vivo magnetic resonance imaging. *Circulation*, *107*(19), 2453–2458.
Lee, H., Lee, E., Kim, D. K., Jang, N. K., Jeong, Y. Y., & Jon, S. (2006). Antibiofouling polymer-coated superparamagnetic iron oxide nanoparticles as potential magnetic resonance contrast agents for in vivo cancer imaging. *Journal of the American Chemical Society*, *128*(22), 7383–7389.
Lee, D.-E., Kim, A., Saravanakumar, G., Koo, H., Kwon, I., Choi, K., et al. (2011). Hyaluronidase-sensitive spions for mr/optical dual imaging nanoprobes. *Macromolecular Research*, *19*(8), 861–867.
Li, A. C., & Glass, C. K. (2002). The macrophage foam cell as a target for therapeutic intervention. *Nature Medicine*, *8*(11), 1235–1242.
Libby, P. (2002). Inflammation in atherosclerosis. *Nature*, *420*(6917), 868–874.
Libby, P., Ridker, P. M., & Maseri, A. (2002). Inflammation and atherosclerosis. *Circulation*, *105*(9), 1135–1143.
Libby, P., DiCarli, M., & Weissleder, R. (2010). The vascular biology of atherosclerosis and imaging targets. *Journal of Nuclear Medicine*, *51*(1 Suppl.), 33S–37S.
Linton, M. F., & Fazio, S. (2001). Class a scavenger receptors, macrophages, and atherosclerosis. *Current Opinion in Lipidology*, *12*(5), 489–495.
MacNeill, B. D., Lowe, H. C., Takano, M., Fuster, V., & Jang, I.-K. (2003). Intravascular modalities for detection of vulnerable plaque. *Arteriosclerosis, Thrombosis, and Vascular Biology*, *23*(8), 1333–1342.
McCarthy, J. R. (2010). Multifunctional agents for concurrent imaging and therapy in cardiovascular disease. *Advanced Drug Delivery Reviews*, *62*(11), 1023–1030.
Paul, K. G., Frigo, T. B., Groman, J. Y., & Groman, E. V. (2004). Synthesis of ultrasmall superparamagnetic iron oxides using reduced polysaccharides. *Bioconjugate Chemistry*, *15*(2), 394–401.
Phinikaridou, A., Ruberg, F. L., Hallock, K. J., Qiao, Y., Hua, N., Viereck, J., et al. (2010). In vivo detection of vulnerable atherosclerotic plaque by mri in a rabbit model/clinical perspective. *Circulation: Cardiovascular Imaging*, *3*(3), 323–332.
Ross, R. (1999). Atherosclerosis—An inflammatory disease. *New England Journal of Medicine*, *340*(2), 115–126.
Sadat, U., Li, Z.-Y., Graves, M. J., Tang, T. Y., & Gillard, J. H. (2009). Noninvasive imaging of atheromatous carotid plaques. *Nature Clinical Practice Cardiovascular Medicine*, *6*(3), 200–209.
Saravanakumar, G., Kim, K., Park, J. H., Rhee, K., & Kwon, I. C. (2009). Current status of nanoparticle-based imaging agents for early diagnosis of cancer and atherosclerosis. *Journal of Biomedical Nanotechnology*, *5*(1), 20–35.
Schatz, C., & Lecommandoux, S. (2010). Polysaccharide-containing block copolymers: Synthesis, properties and applications of an emerging family of glycoconjugates. *Macromolecular Rapid Communications*, *31*(19), 1664–1684.
Schatz, C., Louguet, S., Le Meins, J.-F., & Lecommandoux, S. (2009). Polysaccharide-block-polypeptide copolymer vesicles: Towards synthetic viral capsids13. *Angewandte Chemie International Edition*, *48*(14), 2572–2575.
Shen, L.-H., Zhou, L., Wang, B.-Y., Pu, J., Hu, L.-H., Chai, D.-J., et al. (2008). Oxidized low-density lipoprotein induces differentiation of raw264.7 murine macrophage cell line into dendritic-like cells. *Atherosclerosis*, *199*(2), 257–264.
Sosnovik, D. E., Nahrendorf, M., & Weissleder, R. (2007). Molecular magnetic resonance imaging in cardiovascular medicine. *Circulation*, *115*(15), 2076–2086.
Tassa, C., Shaw, S. Y., & Weissleder, R. (2011). Dextran-coated iron oxide nanoparticles: A versatile platform for targeted molecular imaging, molecular diagnostics, and therapy. *Accounts of Chemical Research*, *44*(10), 842–852.
Trivedi, R. A., U-King-Im, J.-M., Graves, M. J., Cross, J. J., Horsley, J., Goddard, M. J., et al. (2004). In vivo detection of macrophages in human carotid atheroma. *Stroke*, *35*(7), 1631–1635.
Tu, C., Ma, X., Pantazis, P., Kauzlarich, S. M., & Louie, A. Y. (2010). Paramagnetic, silicon quantum dots for magnetic resonance and two-photon imaging of macrophages. *Journal of the American Chemical Society*, *132*(6), 2016–2023.
Tu, C., Ng, T. S. C., Sohi, H. K., Palko, H. A., House, A., Jacobs, R. E., et al. (2011). Receptor-targeted iron oxide nanoparticles for molecular mr imaging of inflamed atherosclerotic plaques. *Biomaterials*, *32*(29), 7209–7216.
Wan, S., Zheng, Y., Liu, Y., Yan, H., & Liu, K. (2005). Fe_3O_4 nanoparticles coated with homopolymers of glycerol mono(meth)acrylate and their block copolymers. *Journal of Materials Chemistry*, *15*(33), 3424–3430.
Wan, S., Huang, J., Yan, H., & Liu, K. (2006). Size-controlled preparation of magnetite nanoparticles in the presence of graft copolymers. *Journal of Materials Chemistry*, *16*(3), 298–303.
Waters, E., & Wickline, S. (2008). Contrast agents for mri. *Basic Research in Cardiology*, *103*(2), 114–121.
Wickline, S. A., Neubauer, A. M., Winter, P. M., Caruthers, S. D., & Lanza, G. M. (2007). Molecular imaging and therapy of atherosclerosis with targeted nanoparticles. *Journal of Magnetic Resonance Imaging*, *25*(4), 667–680.
Yang, L., & Zhang, L.-M. (2009). Chemical structural and chain conformational characterization of some bioactive polysaccharides isolated from natural sources. *Carbohydrate Polymers*, *76*(3), 349–361.
Yoon, H. Y., Saravanakumar, G., Heo, R., Choi, S. H., Song, I. C., Han, M. H., et al. (2012). Hydrotropic magnetic micelles for combined magnetic resonance imaging and cancer therapy. *Journal of Controlled Release*, *160*(3), 692–698.
Zhang, Q., Wang, C., Qiao, L., Yan, H., & Liu, K. (2009). Superparamagnetic iron oxide nanoparticles coated with a folate-conjugated polymer. *Journal of Materials Chemistry*, *19*(44), 8393–8402.